Acta Crystallographica Section F
**Structural Biology and Crystallization Communications**
ISSN 1744-3091

# Structure of the tetradecanucleotide d(CCCCGGTACCGGGG)$_2$ as an A-DNA duplex

**Pradeep Kumar Mandal, Sarkarai Venkadesh and Namasivayam Gautham***

C. A. S. in Crystallography and Biophysics, University of Madras, Guindy, Chennai 600 025, India

Correspondence e-mail: n_gautham@hotmail.com

Received 18 January 2012
Accepted 27 February 2012

**PDB Reference:** d(CCCCGGTACCGGGG)$_2$, 3v9d.

The crystal structure of the tetradecanucleotide sequence d(CCCCGGTACC-GGGG)$_2$ has been determined at 2.5 Å resolution in the tetragonal space group $P4_1$. This sequence was designed with the expectation of a four-way junction. However, the sequence crystallized as an A-DNA duplex and represents more than one full turn of the A-helix. The crystallographic asymmetric unit consists of one tetradecanucleotide duplex. The structural parameters of the A-type DNA duplex structure and the crystal-packing arrangement are described. One $Mn^{2+}$ ion was identified with direct coordination to the N7 position of $G_{13}$ and a water molecule at the major-groove side of the $C_2 \cdot G_{13}$ base pair.

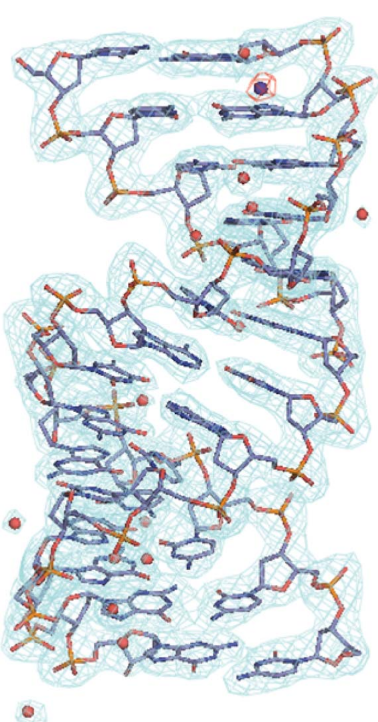



## 1. Introduction

Here, we report the 2.5 Å resolution crystal structure of the tetradecanucleotide invert-repeat sequence d(CCCCGGTACCGGGG)$_2$ in the tetragonal space group $P4_1$. The sequence was designed with (i) an ACC trinucleotide core motif that favours the formation of a right-handed four-way Holliday junction (Eichman *et al.*, 2002; Hays *et al.*, 2003) and (ii) an oligo(dC)·oligo(dG) stretch flanking the trinucleotide core motif that could induce the A-form (Heinemann *et al.*, 1992). The crystals were grown in the presence of $Mn^{2+}$ ions, which were clearly visible in the electron-density maps.

Sequence-dependent conformational features are pronounced in A-DNA in comparison with B-DNA, an observation that is in accord with the notion that A-DNA helices are less malleable (Gao *et al.*, 1995). One or several GpG steps are generally present in A-DNA but are largely absent from B-DNA (Heinemann *et al.*, 1992). Although there are exceptions, it has been suggested that the GpG sequence element could possibly induce or favour the A-form. This finding is in agreement with the results of fibre-diffraction studies of poly(dG)·poly(dC) (Langridge, 1969; Arnott & Selsing, 1974), which prefers the A-form, and with Raman spectroscopic results from G/C-rich oligomers (Benevides *et al.*, 1986).

The crystal structure of the tetradecanucleotide d(CGCGGGT-ACCCGCG)$_2$ in the tetragonal space group $P4_3$ has recently been reported (Venkadesh *et al.*, 2011). Despite the large number of alternating pyrimidine–purine base steps, which favour a Z-type helix, this sequence forms an A-type duplex. In this structure, the asymmetric unit comprised a tetradecanucleotide. Despite sequence symmetry, the structure of the duplex was not symmetrical between the two heptamer halves. Likewise, crystal-packing interactions were not symmetrical for each half of the duplex. The present sequence has a four-nucleotide 'G tract' commonly associated with the A-form (Arnott, 1999). It is interesting to compare the two structures and to deduce possible sequence-dependent microheterogeneity in the helix.

Metal ions are ubiquitous in the crystallization of nucleic acid fragments. These ions promote the close approach of the helices by shielding the negative phosphate charges. Divalent cation-binding sites in the major groove are presently the most extensively studied

**Table 1**
Summary of data-processing and refinement statistics.

Values in parentheses are for the last shell.

| | |
|---|---|
| Diffraction data | |
| Resolution (Å) | 30.0–2.50 (2.59–2.50) |
| Space group | $P4_1$ |
| Unit-cell parameters (Å) | $a = b = 29.34$, $c = 87.69$ |
| $R_{merge}$ (%) | 4.49 (28.24) |
| Mean $I/\sigma(I)$ | 6.6 (1.5) |
| Completeness (%) | 99.7 (99.6) |
| Multiplicity | 4.64 (4.69) |
| No. of observations | 12495 |
| No. of unique reflections | 2599 |
| Refinement | |
| No. of DNA atoms | 568 |
| No. of $Mn^{2+}$ ions | 1 |
| No. of solvent atoms | 15 |
| $R$ factor (%) | 21.6 |
| $R_{free}$ (%) | 24.4 |
| R.m.s.d. bond lengths (°) | 0.02 |
| R.m.s.d. bond angles (Å) | 3.21 |
| Average $B$ factor (Å$^2$) | 33.38 |

class of DNA–counterion interaction (Hud & Polak, 2001). $Mn^{2+}$ ions decrease the melting temperature of DNA and show a destabilizing effect as the (G+C) content of the DNA increases. Using paramagnetic $Mn^{2+}$ as a resonance line-broadening probe in solution-state $^1$H NMR spectroscopy experiments, Sletten and coworkers found that $Mn^{2+}$ binds in the major groove of duplex DNA at GpG, GpA and GpT steps (Frøystein & Sletten, 1991; Frøystein *et al.*, 1993; Sletten & Frøystein, 1996). Crystallographic studies show that divalent cations bind at these same steps and also at the ApG step (Chiu & Dickerson, 2000; Kielkopf *et al.*, 2000). The clear identification of the position of the $Mn^{2+}$ ion in the present structure allows us to supplement the above information regarding the interactions of this ion with DNA.

## 2. Materials and methods

### 2.1. Crystallization, X-ray diffraction data collection and data processing

PAGE-purified DNA oligonucleotides and other chemicals were purchased from Sigma–Aldrich Chemicals Pvt. Ltd (Bangalore, India). Crystallization trials were set up using the hanging-drop vapour-diffusion technique: 1 m*M* DNA, 50–75 m*M* sodium cacodylate trihydrate buffer pH 7.0, 1–15 m*M* $MnCl_2$, 0.5–10 m*M* spermine was equilibrated against 20–50% 2-methyl-2,4-pentanediol (MPD) at 293 K. However, the best crystals (in terms of size and diffraction quality) were obtained from a drop consisting of 1 m*M* DNA, 50 m*M* sodium cacodylate trihydrate buffer pH 7.0, 12 m*M* $MnCl_2$, 10 m*M* spermine equilibrated against 50% MPD. Tetragonal crystals of dimensions 0.1 × 0.1 × 0.2 mm were obtained within 24 h. For data collection at 100 K, one of these crystals was flash-cooled in liquid nitrogen. The mother liquor was sufficient for cryoprotection. X-ray diffraction data were collected in-house on a MAR Research image-plate system using Cu $K\alpha$ radiation ($\lambda$ = 1.5418 Å) generated by a rotating-anode X-ray generator (Bruker AXS) operated at 45 kV

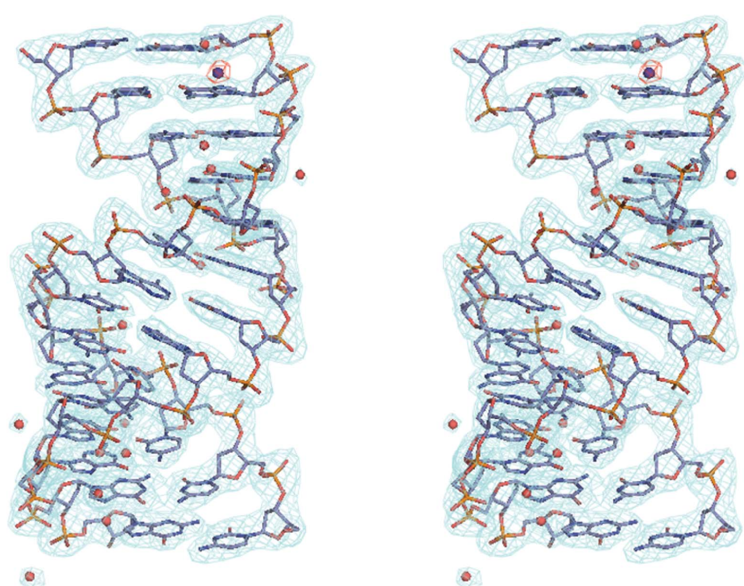

(*a*)

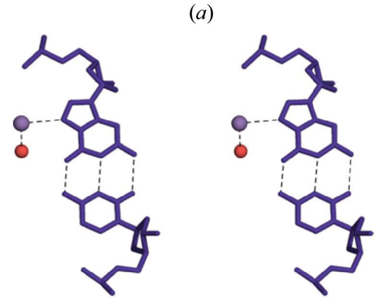

(*b*)

**Figure 1**
Stereoviews of (*a*) the tetradecanucleotide with an anomalous difference Fourier map (red) contoured at the 3$\sigma$ level around $Mn^{2+}$ and a $2F_o - F_c$ map (cyan) contoured at the 1$\sigma$ level and (*b*) the interaction of the $Mn^{2+}$ ion with the N7 atom of $G_{13}$ and a water molecule. $Mn^{2+}$ and solvent atoms are shown as purple and red spheres, respectively.

**Table 2**
Average helical parameters for the present tetradecamer determined using *X3DNA* with respect to both the overall helical axis and the fragmented helical axis and compared with standard values for the description of A-DNA geometry (Olson *et al.*, 2001).

Values in parentheses are standard deviations.

| | d(CCCCGGTACCGGGG)$_2$ (with respect to overall helical axis) | d(CCCCGGTACCGGGG)$_2$ (with respect to fragmented helical axis) | | A-DNA standard value |
|---|---|---|---|---|
| Helical rise (Å) | 3.11 (0.31) | 3.11 (0.44) | 3.13 (0.26) | 2.9 |
| Helical twist (°) | 30.7 (3.8) | 28.7 (2.9) | 30.8 (3.5) | 33.7 |
| Roll (°) | 4.6 (6.2) | 4.4 (7.0) | 5.1 (7.2) | 7.7 |
| Tilt (°) | 0.0 (4.8) | −0.9 (3.3) | −1.6 (6.2) | 0.0 |
| Inclination (°) | 8.5 (11.2) | 8.4 (13.6) | 9.11 (12.1) | 13.7 |
| *X*-displacement (Å) | −4.25 (1.29) | −4.97 (1.01) | −4.29 (1.08) | −3.7 |
| Slide (Å) | −1.76 (0.53) | −2.03 (0.42) | −1.77 (0.51) | −1.42 |
| Major-groove width† (Å) | 5.97 | — | — | 4.19 |
| Minor-groove width† (Å) | 9.54 | 9.56 | 9.53 | 11.28 |
| Intra-strand phosphate–phosphate distance (Å) | 6.00 | 5.99 | 5.96 | 5.57 |
| Sugar puckering | Mostly C3′-*endo* family (C3′-*endo* and C2′-*exo*) | | | |

† Minor-groove and major-groove widths were measured as the 'refined' phosphate–phosphate distances based on the method proposed by El Hassan & Calladine (1998) and incorporated in the program *X3DNA* (Lu & Olson, 2003).

and 60 mA at the G. N. Ramachandran X-ray Diffraction Facility, University of Madras, Chennai, India. Data-collection statistics are given in Table 1.

### 2.2. Structure determination and refinement

The data were processed in space group $P4_1$ with almost identical unit-cell parameters to those of the crystal structure of the sequence d(CGCGGGTACCCGCG)$_2$, which was solved and refined in space group $P4_3$ (Venkadesh *et al.*, 2011). Molecular-replacement trials were carried out with the program *AMoRe* (Navaza, 1994) from the *CCP*4 suite (Winn *et al.*, 2011) using fibre models of A-type, B-type and Z-type DNA (the fibre models were generated using *INSIGHT* II release 98.0; Biosym/MSI, San Diego, USA) for the present tetradecanucleotide in the enantiomeric space groups $P4_1$ and $P4_3$ as well as the higher symmetry space groups $P4_12_12$ and $P4_32_12$. However, the best correlation coefficient (83%) and *R* factor (27%) were consistently obtained using the A-DNA duplex search model in space group $P4_1$.

The Matthews coefficient for data processed in space group $P4_1$ (Matthews, 1968), 2.21 Å$^3$ Da$^{-1}$, indicated that the asymmetric unit was comprised of a duplex. The molecular-replacement solution was subjected to 20 cycles of rigid-body refinement and a further five cycles of restrained refinement in the program *REFMAC*5 (Murshudov *et al.*, 2011). The structure was then refined using *REFMAC*5 with maximum-likelihood targets and the *REFMAC*5 dictionary (Vagin *et al.*, 2004). After initial refinement, a manganese ion was clearly visible at the 5.5$\sigma$ level in the difference Fourier map. Fig. 1(*a*) shows a stereoview of the tetradecanucleotide A-type DNA duplex with an anomalous difference Fourier map confirming the position of the ion and the final $2F_o - F_c$ map. Normally, coordination around $Mn^{2+}$ ions is octahedral. However, the limited resolution of our data set only allowed us to locate one water molecule associated with the $Mn^{2+}$ ion with precision (see Fig. 1*b*). A total of 15 water molecules were added at various stages of the refinement, each time ensuring that the electron density in the $F_o - F_c$ map (and in subsequent maps) as well as the temperature factors in the subsequent cycles of refinement warranted the addition. The final refinement statistics are given in Table 1.

Graphical analyses of the model and the electron-density maps were carried out using *Coot* (Emsley & Cowtan, 2004). Structural analysis and geometrical calculations were carried out using *X3DNA* (Lu & Olson, 2003). *PyMOL* was used to prepare the figures (DeLano, 2002). The coordinates and structure factors have been deposited in the PDB (Berman *et al.*, 2000) with code 3v9d.

## 3. Results and discussion

### 3.1. Overall structure

The crystallographic asymmetric unit consists of a right-handed A-type double helix with Watson–Crick base pairs (see Fig. 1*a*). It had r.m.s.d. values of 1.37 and 1.65 Å when subjected to least-squares superposition of the phosphodiester backbones on the A-DNA fibre model (Arnott & Hukins, 1972) and the tetradecanucleotide duplex d(CGCGGGTACCCGCG)$_2$ (Venkadesh *et al.*, 2011), respectively (see Fig. 2). Table 2 shows the average values of the helical parameters for the d(CCCCGGTACCGGGG)$_2$ duplex calculated with respect to one overall helical axis and to a fragmented axis split at the centre into two axes. The same parameters are also given for a 'standard' A-DNA helix. It is clear from the table that the overall conformation of the d(CCCCGGTACCGGGG)$_2$ helix is that of A-form DNA.

The sequence has twofold symmetry. The r.m.s.d. (least-squares superposition of phosphodiester backbones) of the two halves of the molecule (*i.e.* the first heptamer half superposed on the second heptamer half) is 0.36 Å (see Fig. 3). The heptamers gave r.m.s.d.s of 1.17 and 1.16 Å, respectively, when superposed with the corresponding heptamer of a fibre model of A-type DNA. Thus, the symmetry in the sequence leads to approximate symmetry in the structure of the duplex as well. This is unlike the situation in the other A-type tetradecanucleotide structure d(CGCGGGTACCCGCG)$_2$, in which there is no structural symmetry between the two halves of the duplex (Venkadesh *et al.*, 2011).

In the d(CCCCGGTACCGGGG)$_2$ duplex the values of rise and roll were 3.11 and 4.6 Å, respectively, whereas the d(CGCGGGTACCCGCG)$_2$ duplex was characterized by a low rise (2.47 Å) and a large roll (11.5 Å) (Venkadesh *et al.*, 2011). The low rise and large roll in the latter duplex may be explained by the effect of alternating sequences with CpG steps (Tippin & Sundaralingam, 1996; Wahl & Sundaralingam, 1997; Venkadesh *et al.*, 2011) and crystal packing (Jain & Sundaralingam, 1989).

The d(CCCCGGTACCGGGG)$_2$ duplex is characterized by a wide and shallow minor groove and a deep and narrow major groove (Bingman, Zon *et al.*, 1992). The average minor-groove width is 9.54 Å, which is less than the canonical value of 11.28 Å for A-DNA and the value of 10.38 Å for the d(CGCGGGTACCCGCG)$_2$ duplex.

It is 9.07 Å at its narrowest point and 10.19 Å at its widest point. The average major-groove width is 5.97 Å for the d(CCCCGGTACCGGGG)$_2$ duplex. This is higher than the standard value of 4.19 Å for A-DNA and the value of 3.26 Å for the d(CGCGGGTACCCGCG)$_2$ duplex. It is 5.24 Å at its narrowest point and 7.00 Å at the widest point. The average intra-strand phosphate–phosphate distance is 6.00 Å, as in canonical A-DNA, with a range from 5.43 to 6.71 Å.

### 3.2. Helical axes and analysis of local helical bending

Previous A-DNA dodecamer structures indicated that the overall helical axis may be inadequate to calculate helical parameters for long sequences (Bingman, Jain *et al.*, 1992; Bingman, Zon *et al.*, 1992). In order to verify this, helical parameters were calculated with respect to the overall helical axis as well with respect to the axis fragmented in two, with base pairs 1–7 forming one fragment and base pairs 8–14 forming the other. Table 2 shows the two sets of parameters. There is no significant deviation between these values and those calculated using the single overall helix axis. The present duplex is straight, without any bend or kink.

### 3.3. Crystal packing

The crystal structures of A-DNA duplexes exhibit a typical packing pattern in which the terminal base pair of one helix abuts or stacks on the shallow minor groove of a symmetry-related neighbouring helix (Wahl & Sundaralingam, 1997). In other DNA forms such as B-form and Z-form DNA and in RNA the approximately cylindrical duplexes typically stack coaxially on top of each other (Wahl & Sundaralingam, 1997). Although the above packing pattern is found in all A-DNA crystals, the exact nature of the interaction between the symmetry-related duplexes varies, apparently with sequence length and space group (Wahl & Sundaralingam, 1997). It has been observed

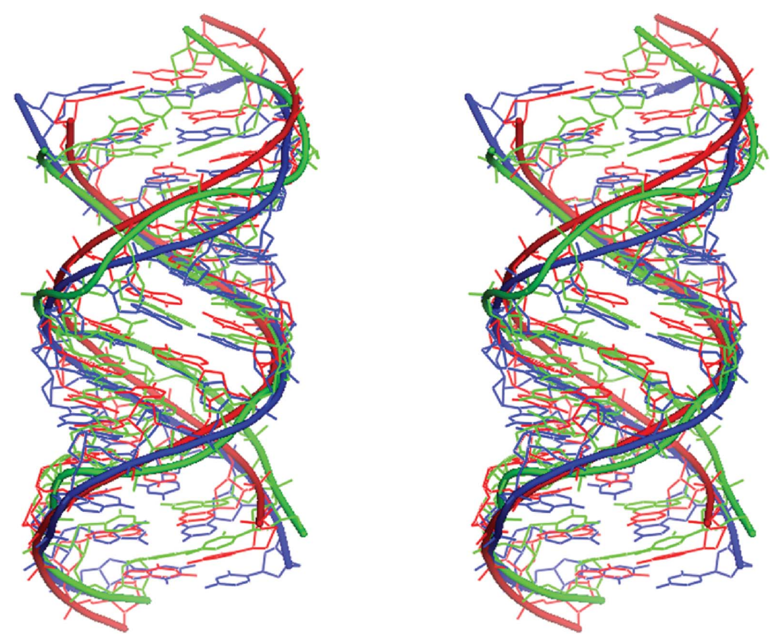

**Figure 2**
Stereoview of least-squares superposition of the present tetradecanucleotide structure (blue) on the A-DNA fibre model (red; Arnott & Hukins, 1972) and the A-DNA tetradecanucleotide duplex d(CGCGGGTACCCGCG)$_2$ (green; Venkadesh *et al.*, 2011).

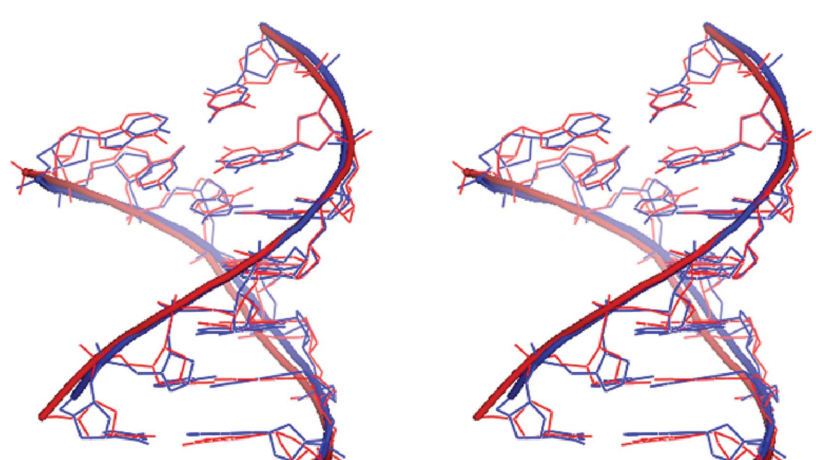

**Figure 3**
Stereoview of least-squares superposition of one half of the tetradecanucleotide (heptamer 1; red) onto the other half (heptamer 2; blue).

that A-DNA octamers that contain a central pyrimidine–purine step mostly crystallize in tetragonal space groups (Tippin & Sundaralingam, 1996). In the case of d(CGCGGGTACCCGCG)$_2$ (Venkadesh *et al.*, 2011) the helices are in the left-handed ($P4_3$) screw-axial arrangement (see Fig. 4*a*), whereas the present tetradecanucleotide (which contains a central TpA step) crystallizes in space group $P4_1$ and has a right-handed screw-axial arrangement (see Fig. 4*b*). The two tetradecanucleotide helices are in an enantiomeric screw-axial arrangement and a possible explanation for this can be obtained by analyzing the crystal-packing interactions.

In the previous tetradecanucleotide structure (Venkadesh *et al.*, 2011) the asymmetric unit makes five major types of contacts with symmetry-related helices. These interactions are (i) minor groove to minor groove, (ii) minor groove to backbone, (iii) backbone to

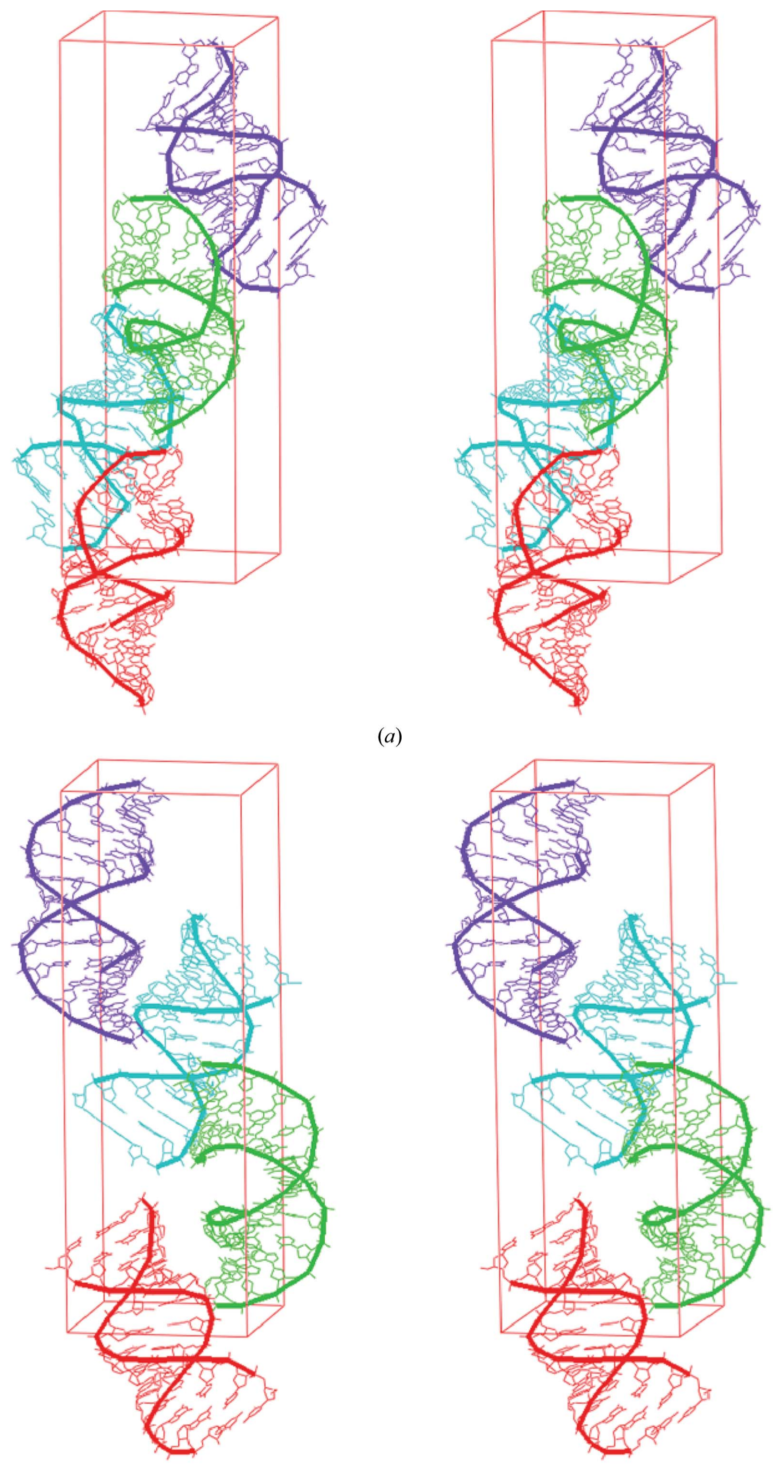

(*a*)

(*b*)

**Figure 4**
Stereoviews of the arrangement of A-DNA helices in the unit cells of (*a*) d(CGCGGGTACCCGCG)$_2$ (Venkadesh *et al.*, 2011) and (*b*) d(CCCCGGTACCGGGG)$_2$. Unit cells are shown as lines.

backbone type 1, (iv) backbone to backbone type 2 and (v) terminal base pair to minor groove. Of these five types of interactions, (i) and (ii) arose from alternating sequence-based modulations that give rise to different types of crystal-packing contacts. These interactions gave rise to perturbations in the helical parameters: (i) the base pair $C_1 \cdot G_{28}$ has high buckle (16.1°), propeller (26.9°) and opening (−14.5°) and (ii) the base pair $C_1 \cdot G_2/C_3 \cdot G_4$ has high inclination (33.9°) and large helical twist (64.4°), making the minor groove of the first base-pair exposed to the minor groove and backbone of the neighbouring helix. These minor-groove-based packing interactions might contribute to the left-handed screw-axial arrangement of the helices. However, in the present tetradecanucleotide structure the minor groove to minor groove and minor groove to backbone interactions are absent. This may be a consequence of the lack of alternating sequence-dependent modulations. The 'G tract' in the present sequence thus appears to limit the minor-groove exposure, with a consequent absence of these packing interactions.

### 3.4. Ion interactions

In general, $Mn^{2+}$ ions interact with DNA by coordinating to the N7 position of purines, especially that of guanine (Saenger, 1984). Previous reports have demonstrated that AT-rich sequences localize monovalent and divalent cations in a sequence-specific manner in the minor groove (Hud & Feigon, 1997; Hud *et al.*, 1999). An analysis of divalent cations in a number of high-resolution DNA crystal structures revealed that divalent cations can be bound at the top of a minor groove for DNA sequence elements with a narrow minor groove (*e.g.* AATT; Minasov *et al.*, 1999; Tereshko *et al.*, 1999; Sines *et al.*, 2000). $Mn^{2+}$ ions have been localized in the minor groove of the sequence elements $A_4T_4$ and $T_4A_4$ in the dodecamer duplexes $[d(GCA_4T_4GC)]_2$ and $[d(CGT_4A_4CG)]_2$, respectively (Hud & Feigon, 2002).

In the present structure, one $Mn^{2+}$ ion is clearly visible at the major-groove side of the $C_2 \cdot G_{13}$ base pair, with direct coordination to the N7 position of $G_{13}$ and a water molecule (see Figs. 1). Normally, the coordination around an $Mn^{2+}$ ion is octahedral. The limited resolution of our data set does not allow us to locate the water molecules associated with $Mn^{2+}$ ions with precision, except for one. The N7—$Mn^{2+}$ distance is 2.84 Å. The water molecule is positioned at a distance of 2.43 Å from the ion. The N7–$Mn^{2+}$–water molecule angle is ∼100°. The metal-ion interaction does not alter the A-DNA structure significantly.

In B-type duplexes, for example the oligonucleotide $d(CGTTAATTAACG)_2$ crystallized in the presence of $Mn^{2+}$ (10 m*M*) and a low spermine concentration (0.25 m*M*) (Millonig *et al.*, 2009), the ions form direct bridges between neighbouring duplexes in the crystal. However, this type of direct bridging is absent in the present A-type duplex. The present tetradecanucleotide has sequence symmetry with one $Mn^{2+}$ ion in the major-groove side of $C_2 \cdot G_{13}$ of the first heptamer half. However, the ion is absent in the vicinity of the second heptamer half. Possible explanations for the absence of the ion in the second heptamer half may be that (i) electrostatic repulsions apparently do not allow two $Mn^{2+}$ ions to simultaneously occupy two symmetry-related and closely spaced cation-binding sites in the crystal state (Chiu & Dickerson, 2000; Kielkopf *et al.*, 2000) and (ii) the high concentration of spermine used in the crystallization condition may reduce the association of $Mn^{2+}$ ions in the present structure.

### 3.5. Hydration

About ten water molecules per base pair can be located in the electron density of an average A-DNA crystal structure, although the crystals usually have a solvent content of about 50% (Wahl & Sundaralingam, 1997). However, in the present case we could not carry out any detailed analysis on this basis. In the present case, 15 water molecules were located in the electron density (see Fig. 1*a*). The central TpA step is not hydrated on both the major-groove and minor-groove sides.

To summarize, this crystallographic study of the tetradecanucleotide sequence provides a view of more than one full turn of an A-helix. Despite the sequence being designed to form a four-way junction structure with an ACC core motif, it forms an A-type duplex. The presence of a TpA step at the core does not induce a kink or a bend when the present tetradecanucleotide is compared with the first full turn of the structure of the tetradecanucleotide $d(CGCGGGTACCGCG)_2$ reported previously (Venkadesh *et al.*, 2011) and structural differences are observed. However, the overall structure of the present tetradecanucleotide structure is similar to the fibre model, with minor local variations. Despite possessing sequence symmetry, each half the duplex possesses a different set of inter-helical contacts with symmetry-related helices. The $Mn^{2+}$ ion shows direct interaction with the N7 atom of $G_{13}$ ($C_2 \cdot G_{13}$ of the first heptamer half) and does not alter the normal conformational parameters for the A-form. However, the ion is absent in the vicinity of the second heptamer half.

We gratefully acknowledge financial assistance from the following agencies of the Government of India: DBT for research grants, DST for grants under the FIST programme and UGC for grants under the CAS program. PKM and SV thank CSIR for Senior Research Fellowships.

## References

Arnott, S. (1999). *Oxford Handbook of Nucleic Acid Structure*, edited by S. Neidle, pp. 1–38. Oxford University Press.
Arnott, S. & Hukins, D. W. (1972). *Biochem. Biophys. Res. Commun.* **47**, 1504–1509.
Arnott, S. & Selsing, E. (1974). *J. Mol. Biol.* **88**, 551–552.
Benevides, J. M., Wang, A. H.-J., Rich, A., Kyogoku, Y., van der Marel, G. A., van Boom, J. H. & Thomas, G. J. (1986). *Biochemistry*, **25**, 41–50.
Berman, H. M., Westbrook, J., Feng, Z., Gilliland, G., Bhat, T. N., Weissig, H., Shindyalov, I. N. & Bourne, P. E. (2000). *Nucleic Acids Res.* **28**, 235–242.
Bingman, C., Jain, S., Zon, G. & Sundaralingam, M. (1992). *Nucleic Acids Res.* **20**, 6637–6647.
Bingman, C., Zon, G. & Sundaralingam, M. (1992). *J. Mol. Biol.* **227**, 738–756.
Chiu, T. K. & Dickerson, R. E. (2000). *J. Mol. Biol.* **301**, 915–945.
DeLano, W. L. (2002). *PyMOL.* http://www.pymol.org.
Eichman, B. F., Ortiz-Lombardía, M., Aymamí, J., Coll, M. & Ho, P. S. (2002). *J. Mol. Biol.* **320**, 1037–1051.
El Hassan, M. A. & Calladine, C. R. (1998). *J. Mol. Biol.* **282**, 331–343.
Emsley, P. & Cowtan, K. (2004). *Acta Cryst.* D**60**, 2126–2132.
Frøystein, N. A., Davis, J. T., Reid, B. R. & Sletten, E. (1993). *Acta Chem. Scand.* **47**, 649–657.
Frøystein, N. A. & Sletten, E. (1991). *Acta Chem. Scand.* **45**, 219–225.
Gao, Y. G., Robinson, H., van Boom, J. H. & Wang, A. H. (1995). *Biophys. J.* **69**, 559–568.
Hays, F. A., Watson, J. & Ho, P. S. (2003). *J. Biol. Chem.* **278**, 49663–49666.
Heinemann, U., Alings, C. & Bansal, M. (1992). *EMBO J.* **11**, 1931–1939.
Hud, N. V. & Feigon, J. (1997). *J. Am. Chem. Soc.* **119**, 5756–5757.
Hud, N. V. & Feigon, J. (2002). *Biochemistry*, **41**, 9900–9910.
Hud, N. V. & Polak, M. (2001). *Curr. Opin. Struct. Biol.* **11**, 293–301.
Hud, N. V., Sklenár, V. & Feigon, J. (1999). *J. Mol. Biol.* **286**, 651–660.
Jain, S. & Sundaralingam, M. (1989). *J. Biol. Chem.* **264**, 12770–12784.
Kielkopf, C. L., Ding, S., Kuhn, P. & Rees, D. C. (2000). *J. Mol. Biol.* **296**, 787–801.
Langridge, R. (1969). *J. Cell. Physiol.* **74**, Suppl. 1, 1–20.
Lu, X.-J. & Olson, W. K. (2003). *Nucleic Acids Res.* **31**, 5108–5121.
Matthews, B. W. (1968). *J. Mol. Biol.* **33**, 491–497.
Millonig, H., Pous, J., Gouyette, C., Subirana, J. A. & Campos, J. L. (2009). *J. Inorg. Biochem.* **103**, 876–880.

Minasov, G., Tereshko, V. & Egli, M. (1999). *J. Mol. Biol.* **291**, 83–99.
Murshudov, G. N., Skubák, P., Lebedev, A. A., Pannu, N. S., Steiner, R. A., Nicholls, R. A., Winn, M. D., Long, F. & Vagin, A. A. (2011). *Acta Cryst.* D**67**, 355–367.
Navaza, J. (1994). *Acta Cryst.* A**50**, 157–163.
Olson, W. K. *et al.* (2001). *J. Mol. Biol.* **313**, 229–237.
Saenger, W. (1984). *Principles of Nucleic Acid Structure*, pp. 201–219. New York: Springer-Verlag.
Sines, C. C., McFail-Isom, L., Howerton, S. B., Van Derveer, D. & Williams, L. D. (2000). *J. Am. Chem. Soc.* **122**, 11048–11056.
Sletten, E. & Frøystein, N. A. (1996). *Metal Ions in Biological Systems*, edited by A. Sigel & H. Sigel, pp. 397–418. New York: Dekker.
Tereshko, V., Minasov, G. & Egli, M. (1999). *J. Am. Chem. Soc.* **121**, 3590–3595.
Tippin, D. B. & Sundaralingam, M. (1996). *Acta Cryst.* D**52**, 997–1003.
Vagin, A. A., Steiner, R. A., Lebedev, A. A., Potterton, L., McNicholas, S., Long, F. & Murshudov, G. N. (2004). *Acta Cryst.* D**60**, 2184–2195.
Venkadesh, S., Mandal, P. K. & Gautham, N. (2011). *Biochem. Biophys. Res. Commun.* **407**, 307–312.
Wahl, M. C. & Sundaralingam, M. (1997). *Biopolymers*, **44**, 45–63.
Winn, M. D. *et al.* (2011). *Acta Cryst.* D**67**, 235–242.